δ^*_{MM}–π_L Odd Electron Delocalization onto Aromatic Bridging Ligands in a Paramagnetic Dirhodium Complex and Intermolecular π-Stack Interaction in Crystal

Takashi Kawamura,* Hisanori Kachi, Hiroshi Fujii, Chihiro Kachi-Terajima, Yuzuru Kawamura, Naohiro Kanematsu, Masahiro Ebihara,† Kunihisa Sugimoto,†† Takayoshi Kuroda-Sowa,†† and Megumu Munakata ††

Department of Chemistry, Faculty of Engineering, Gifu University, Yanagido, Gifu 501-1193

†Institute for Molecular Science, Myodaiji, Okazaki 444-8585

††Department of Chemistry, Kinki University, Kowakae, Higashi-Osaka, Osaka 577-8502

(Received September 21, 1999)

The odd electron in the δ^*_{RhRh} orbital of (3,1)-$[Rh_2(mhq)_4py]^+$ ($\mathbf{1}^+$; Hmhq = 4-methyl-2-quinolinol) was estimated to be delocalized onto each π system of the four mhq bridges to the extent of ca. 9% based on its ^{1}H NMR paramagnetic shifts. The experimental spin distribution in the mhq ligands is consistent with a model of mixing of the π HOMOs of the mhq ligands into the δ^*_{RhRh} singly occupied molecular orbital (SOMO). In crystals of (3,1)-$[Rh_2(hq)_4py]$ (**2**; Hhq = 2-quinolinol) and its cationic radical salts, **2** or $\mathbf{2}^+$ molecules form intermolecular π-stack arrangements of hq ligands. Intermolecular interaction between $\mathbf{2}^+$ molecules in crystal was studied by examining electronic spectra, magnetic susceptibility, ESR, and electrical conductance of its salts.

Mixing of δ_{MM}- or δ^*_{MM}-type orbitals with π orbitals of bridging ligands in a lantern-type dinuclear complex has attracted attention in studies of the ligand dependence of the electron configuration for the M_2 core, M–L electron delocalization, and intramolecular electronic interactions between two or more of M_2 cores through bridging ligand(s) in $(M_2)_n$-type complexes.[1–8] The δ^*_{MM} orbital of lantern-type dinuclear complexes is in phase with the π HOMO of bridging ligands with four π electrons such as carboxylates and amidates, so enhanced interactions between these orbitals are expected. The odd electron in a Rh_2^{5+} complex with π donating bridging ligands such as anions of *o*-hydroxypyridines and amides is accommodated in the δ^*_{RhRh} orbital.[4,9] If the mixing of the δ^*_{RhRh} SOMO and π_{bridge} orbitals takes place to a chemically significant extent, the SOMO should have a sterically interesting shape, as symbolically depicted in Scheme 1a.[10] Density functional theory (DFT) calculations of $[Rh_2(HNCHO)_4(H_2O)_2]^+$ and $[Rh_2(HNCHNH)_4]^+$ have shown that the spin population in each of their bridging ligands would be around 0.1.[11] Intermolecular π-stack interactions between aromatic bridging ligands of this type of complex in a crystal would form 1- to 3-dimensional electronic interaction systems (Scheme 1b). To examine this possibility, we prepared salts of $\mathbf{1}^+$ and $\mathbf{2}^+$, which we found stable and easy to handle.

In this report, we examine paramagnetic shifts in ^{1}H NMR of $\mathbf{1}^+$ to estimate the extent of the δ^*_{RhRh}–π_{bridge} odd electron delocalization. The methyl substituent in the bridging ligand

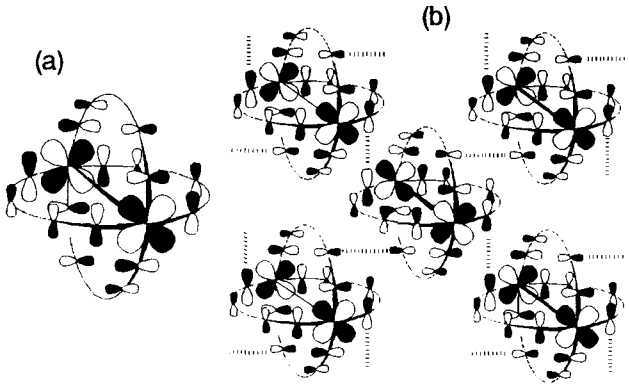

Scheme 1.

was introduced to help the assignment of ^{1}H NMR peaks and to increase the solubility of the complex. We study also crystal structures, magnetic susceptibilities, electronic absorption and ESR spectra, and electrical conductivities of crystalline salts of $\mathbf{2}^+$ to examine effects of intermolecular electronic interaction between frontier electrons in the metal cores induced by the intramolecular δ^*_{RhRh}–π_{bridge} electron delocalization and the intermolecular π-stack interaction in crystal.

Experimental

General Methods. Preparations of Rh_2 complexes were carried out under argon atmosphere by using standard Shlenk techniques. Infrared spectra were recorded on a Perkin–Elmer 1600 FT-IR

spectrophotometer in KBr pellets. UV-vis absorption spectra were measured on a Hitachi U-3500 spectrophotometer. Electronic absorption spectra of finely powdered crystalline salts were measured as nujol mulls between quartz discs. NMR spectra were recorded on JEOL Alpha-400 and Varian Inova 500 FT-NMR spectrometers. ESR spectra were recorded on a JEOL JES TE-200 spectrometer. Field sweep was monitored with an Echo Electronics EFM-2000 ^{1}H NMR gaussmeter, the probe of which was attached beside the ESR cavity. The field difference between the ESR and NMR sample positions was calibrated by measuring the field intensity at the resonance of perylene cationic radical in concd H_2SO_4 (g = 2.002583).[12] Cyclic voltammograms (CVs) were observed by using a BAS Pt disk working electrode and a Pt wire counter electrode. The potential measured relative to a BAS RE-5 reference electrode (Ag^+/Ag/CH_3CN) was converted into that relative to the Fc^+/Fc potential as described previously.[13] Magnetic susceptibilities were measured by using a Quantum Design MPMS2 SQUID magnetometer. The applied magnetic field was 1 T. Observed susceptibilities were corrected for diamagnetic susceptibilities based on the experimental magnetic susceptibility of the diamagnetic compound, **2**·1.5CH_2ClCH_2Cl ($\chi_{mol} = 442.1\times10^{-6}$ emu mol^{-1} at 270 K), and the Pascal rule.[14,15] X-Ray powder diffraction patterns were measured on a Rigaku Geigerflex 2013 diffractometer using Cu $K\alpha$ radiation. Electrical conductivities were measured by using an Advantest R6441A digital multimeter and gold-plated probes with a two-terminal method. Elemental analyses were performed at the Elemental Analysis Center of Kyoto University.

Materials. [$Rh_2(OAc)_4$] was prepared by following a literature method.[16] Diglyme and toluene were distilled over $LiAlH_4$. Dichloromethane, 1,2-dichloroethane, *o*-dichlorobenzene and hexane were distilled from P_2O_5. Pyridine was dried over KOH and distilled. Methanol, acetonitrile and carbon tetrachloride were dried with molecular sieves.

(3,1)-[Rh_2(mhq)$_4$py] (1). A mixture of [$Rh_2(OAc)_4$] (1.00 g, 2.26 mmol) and Hmhq (2.88 g, 18.1 mmol) in 70 ml of diglyme was refluxed for 19 h. A yellow-green precipitate which formed during heating was separated by filtration, washed with hot methanol and dried in vacuo. The precipitate was dissolved into refluxing acetonitrile (5 dm^3) and filtered. After evaporation of the solvent, the residual solid was chromatographed on a silica-gel column (eluent 1,2-dichloroethane added with 5 vol% of acetonitrile). The third colored band (green) was collected, and the solvent was removed in vacuo. The green residue was dissolved in pyridine to give a red-purple solution and evaporated to dryness. Recrystallization of the residual solid from pyridine–toluene (1 : 1 by v/v) afforded **1** as purple microcrystals (0.504 g, 0.549 mmol, 24% yield). IR (KBr, cm^{-1}): 1619 (s), 1555 (m), 1499 (s), 1430 (s), 1411 (s), 1208 (m), 1019 (w), 870 (w), 752 (m), 696 (w), 670 (w), 644 (w). UV-vis [CH_2Cl_2, λ_{max}/nm (log ε)] 303 (4.57), 448 (sh), 560 (2.58). ^{1}H NMR (400 MHz, CD_2Cl_2; see the section of Results and Discussion for the numbering of protons and assignment of the resonances) δ = 9.25 (2H (H_{8C}), d, J ($H_{8C}H_{7C}$) = 8.4 Hz), 9.02 (2H ($H_{py\text{-}o}$), d, J ($H_{py\text{-}o}H_{py\text{-}m}$) = 4.8 Hz), 8.80 (1H ($H_{8B}$), br d, J ($H_{8B}H_{7B}$) = 8.2 Hz), 8.01 (1H ($H_{py\text{-}p}$), t, J ($H_{py\text{-}p}H_{py\text{-}m}$) = 7.6 Hz), 7.66 (2H ($H_{7C}$), ddd, J ($H_{8C}H_{7C}$) = 8.4 Hz, J ($H_{7C}H_{6C}$) = 7.2 Hz, J ($H_{7C}H_{5C}$) = 1.2 Hz), 7.58 (2H (H_{5C}), dd, J ($H_{5C}H_{6C}$) = 8.0 Hz, J ($H_{7C}H_{5C}$) = 1.2 Hz), 7.57 (2H ($H_{py\text{-}m}$), br t, J = ca. 6 Hz), 7.53 (1H (H_{8A}), dd, J ($H_{8A}H_{7A}$) = 8.2 Hz, J ($H_{8A}H_{6A}$) = 1.2 Hz), 7.46 (1H (H_{5B}), dd, J ($H_{5B}H_{6B}$) = 8.2 Hz, J ($H_{7B}H_{5B}$) = 1.4 Hz), 7.42 (1H (H_{5A}), dd, J ($H_{5A}H_{6A}$) = 8.2 Hz, J ($H_{7A}H_{5A}$) = 1.4 Hz), 7.28 (1H (H_{7B}), ddd, J ($H_{8B}H_{7B}$) = 8.2 Hz, J ($H_{7B}H_{6B}$) = 7.0 Hz, J ($H_{7B}H_{5B}$) = 1.4 Hz), 7.17 (2H (H_{6C}), ddd, J ($H_{6C}H_{5C}$) = 8.0 Hz, J ($H_{7C}H_{6C}$) = 7.2 Hz, J ($H_{7C}H_{5C}$) = 1.2 Hz), 7.00 (1H (H_{6B}), ddd, J ($H_{6B}H_{5B}$) = 8.2 Hz, J ($H_{7B}H_{6B}$) = 7.0 Hz, J ($H_{6B}H_{8B}$) = 1.2 Hz), 6.90 (1H (H_{6A}), ddd, J ($H_{6A}H_{5A}$) = 8.2 Hz, J ($H_{7A}H_{6A}$) = 7.2 Hz, J ($H_{8A}H_{6A}$) = 1.2 Hz), 6.83 (1H (H_{7A}), ddd, J ($H_{8A}H_{7A}$) = 8.2 Hz, J ($H_{7A}H_{6A}$) = 7.2 Hz, J ($H_{7A}H_{5A}$) = 1.4 Hz), 6.37 (3H (H_{3B}, H_{3C}), br s), 6.21 (1H (H_{3A}), br s), 2.28 (6H (CH_3)$_C$, br s), 2.27 (6H (CH_3)$_A$ and (CH_3)$_B$, br s). Calcd for $C_{45}H_{37}N_5O_4Rh_2$: C, 58.90; H, 4.06; N, 7.63%. Found: C, 58.62; H, 4.15; N, 7.58%.

(3,1)-[Rh_2(mhq)$_4$(py-d^5)] (**1**-d^5) for the assignment of the resonances of the pyridine protons and for a two-dimensional nuclear Overhauser effect NMR spectroscopy (NOESY) study was prepared by dissolving **1** into C_5D_5N followed by evaporation of the solvent.

(3,1)-[Rh_2(hq)$_4$py]·1.5CH_2ClCH_2Cl (2·1.5CH_2ClCH_2Cl). A mixture of [$Rh_2(OAc)_4$] (1.10 g, 2.29 mmol) and Hhq (2.64 g, 18.2 mmol) in 14 ml of diglyme was refluxed for 1 d. A yellow solid formed during reflux was filtered, washed with hot methanol, and refluxed in pyridine for 1 h to give deep red solution. After evaporation of the solvent, the red solid was chromatographed on a silica-gel column (eluent: 1,2-dichloroethane). The second band (purple) was collected and evaporated to dryness. The residue was dissolved in 1,2-dichloroethane and recrystallized by slow diffusion of *n*-hexane to give deep red microcrystals of **2**·1.5CH_2ClCH_2Cl (1.16 g, 1.15 mmol) in 50% yield. IR (KBr), 1618 (s), 1560 (m), 1508 (s), 1488 (m), 1481 (m), 1460 (m), 1449 (w), 1427 (s), 1401 (s), 1389 (s), 1314 (m), 1214 (m), 1124 (m), 825 (s), 752 (s), 694 (m), 646 (w), 616 (m), 475 cm^{-1} (m). UV-vis [C_5H_5N, λ_{max}/nm (log ε)] 304 (4.52), 457 (sh), 557 (2.60). ^{1}H NMR (400 MHz, $CDCl_3$) δ = 9.21 (2H, d, J = 8.4 Hz), 9.04 (2H, d, J = 4.8 Hz), 8.75 (1H, d, J = 8.0 Hz), 8.02 (1H, t, J = 7.6 Hz), 7.67 (2H, t, J = 7.8 Hz), 7.59 (2H, t, J = 6.8 Hz), 7.44 (7H, m), 7.29 (3H, m), 7.16 (2H, t, J = 8.0 Hz), 6.99 (1H, t, J = 7.8 Hz), 6.87 (2H, m), 6.50 (1H, d, J = 8.8 Hz), 6.49 (2H, d, J = 8.8 Hz), 6.32 (1H, d, J = 8.8 Hz). Calcd for $C_{44}H_{35}Cl_3N_5O_4Rh_2$: C, 52.33; H, 3.49; N, 6.93%. Found: C, 52.33; H, 3.37; N, 6.96%.

(3,1)-[Rh_2(mhq)$_4$py]PF_6·(1/3)CH_2ClCH_2Cl (3) and (3,1)-[Rh_2(mhq)$_4$py]PF_6·2CH_2ClCH_2Cl (4). To **1** (0.318 g, 0.347 mmol) in 50 ml of 1,2-dichloroethane, dry $AgPF_6$ (0.178 g, 0.704 mmol) suspended in 30 ml of 1,2-dichloroethane was added at 0 °C. The mixture was stirred for 10 min. The metallic silver precipitate was filtered off and the solvent was removed from the filtrate. The residue was washed with toluene to remove the excess of $AgPF_6$ and recrystallized by dissolving in 1,2-dichloroethane followed by slow diffusion of hexane to give dark blue microcrystals. The microcrystals were shown to be (3,1)-[Rh_2(mhq)$_4$py]-PF_6·2CH_2ClCH_2Cl (**4**) by an X-ray structure analysis at −80 °C (vide infra) but they lose solvate molecules quickly in open air at room temperature. The cationic radical salt with a stable composition (namely, **3**) was obtained by vacuum drying of **4** for 70 h at room temperature (0.099 g, 0.090 mmol, 26% yield). IR of **3** (KBr), 1654 (w), 1618 (s), 1560 (w), 1500 (s), 1411 (m), 1346 (w), 1209 (w), 1020 (w), 843 (s), 757 (w), 670 (w), 558 cm^{-1} (w). Calcd for $C_{137}H_{115}Cl_2F_{18}N_{15}O_{12}P_3Rh_6$: C, 50.06; H, 3.53; N, 6.39%. Found: C, 49.89; H, 3.56; N, 6.43%.

(3,1)-[Rh_2(hq)$_4$py]$SbCl_6$·CH_2Cl_2 (5). To **2**·1.5CH_2ClCH_2Cl (0.594 g, 0.588 mmol) in 100 ml of dichloromethane, [N(*p*-$BrC_6H_4)_3$]$SbCl_6$ (0.478 g, 0.586 mmol) in 80 ml of dichloromethane was added at 0 °C. The mixture was stirred for 10 min. After evaporation of the solvent, the residue was washed with toluene to remove [N(*p*-$BrC_6H_4)_3$]. The blue solid was dissolved in 100 ml of acetonitrile and this solution was filtered. The filtrate was evaporated to dryness and the blue residue was recrystallized by

layering *n*-hexane on its dichloromethane solution to give greenish blue crystals of **5** (0.62 g, 0.49 mmol) in 83% yield. IR (KBr), 1606 (m), 1560 (w), 1504 (s), 1426 (s), 1369 (m), 1318 (s), 1214 (w), 1124 (w), 825 (m), 754 cm^{-1} (s). UV-vis [CH_2Cl_2, λ_{max}/nm (log ε)] 274 (4.85), 541 (sh), 678 (3.38), 922 (3.86), 1063 (sh). Calcd for $C_{42}H_{31}Cl_8N_5O_4Rh_2Sb$: C, 39.38; H, 2.44; N, 5.47%. Found: C, 39.11; H, 2.43; N, 5.35%.

(3,1)-[Rh_2(hq)$_4$py]PF_6·2*o*-$C_6H_4Cl_2$ (6). To **2**·1.5CH_2ClCH_2-Cl (0.145 g, 0.144 mmol) in 30 ml of dichloromethane, dry $AgPF_6$ (0.047 g, 0.19 mmol) suspended in 30 ml of dichloromethane was added at 0 °C. This mixture was stirred for 10 min. The metallic silver precipitate was filtered off. After evaporation of the solvent, the residue was washed with toluene. The residue was dissolved into a small amount of *o*-dichlorobenzene and recrystallized by slow diffusion of *n*-hexane to give dark blue crystals of **6** (0.12 g, 0.088 mmol) in 61% yield. IR (KBr), 1618 (m), 1560 (w), 1508 (s), 1429 (s), 1400 (w), 1388 (w), 1318 (m), 1214 (w), 1125 (w), 842 (s), 755 (m), 559 cm^{-1} (m). UV-vis [CH_2Cl_2, λ_{max}/nm (log ε)] 276 (4.52), 545 (sh), 678 (3.38), 929 (3.87), 1051 (sh). Calcd for $C_{53}H_{37}Cl_4F_6N_5O_4PRh_2$: C, 48.95; H, 2.87; N, 5.39%. Found: C, 48.90; H, 2.92; N, 5.46%.

(3,1)-[Rh_2(hq)$_4$py]PF_6 (7). Cationic radical salt **6** was dissolved into dichloromethane–methanol (1 : 1 v/v), on which *n*-hexane was layered to give dark blue crystals of **7**. IR (KBr), 1618 (m), 1560 (m), 1508 (s), 1426 (s), 1380 (m), 1342 (m), 1320 (m), 981 (w), 851 (s), 752 (m), 558 cm^{-1} (m). Calcd for $C_{41}H_{29}F_6N_5O_4PRh_2$: C, 48.93; H, 2.90; N, 6.96%. Found: C, 48.73; H, 3.00; N, 6.88%.

(3,1)-[Rh_2(hq)$_4$py]CF_3SO_3·2CH_2ClCH_2Cl (8). **2**·1.5CH_2-$ClCH_2Cl$ (0.477 g, 0.472 mmol) was oxidized by dry CF_3SO_3Ag (0.377 g, 1.47 mmol) similarly to the procedure for the preparation of **6**. The cationic radical salt was recrystallized by slow diffusion of carbon tetrachloride into a 1,2-dichloroethane solution of the salt to give dark blue crystals of **8** (0.40 g, 0.33 mmol) in 70% yield. Crystal **8** loses solvate molecules very slowly in open air at room temperature. IR (KBr), 1618 (m), 1560 (m), 1508 (s), 1427 (s), 1388 (w), 1342 (w), 1318 (m), 1260 (m), 1156 (w), 1037 (m), 824 (m), 754 (m), 638 cm^{-1} (m). Calcd for $C_{46}H_{37}Cl_4F_3N_5O_7Rh_2S$: C, 45.72; H, 3.09; N, 5.80%. Found: C, 45.72; H, 3.31; N, 5.62%.

X-Ray Crystallography. A prismatic deep red single crystal of **2**·1.5CH_2ClCH_2Cl for an X-ray structure study was obtained by slow diffusion of *n*-hexane into a 1,2-dichloroethane solution of the complex. A prismatic dark blue single crystal of **4** was grown by layering *n*-hexane on a CH_2ClCH_2Cl solution of **3**. The crystal loses solvate molecules at room temperature, but it was stable at −80 °C and X-ray diffraction data were collected at this temperature. Single crystals of **5**—**8** were grown by careful and slow recrystallization of these salts by using the solvents described in the section about their preparation.

The diffraction data were collected on a Rigaku AFC-7R diffractometer using graphite monochromated Mo $K\alpha$ radiation (λ = 0.71069 Å). Low temperature data collections were performed for crystals in a cold nitrogen gas flow controlled by a Rigaku XR-TCS-2-050 temperature controller. The positions of heavy atoms in **2**·1.5CH_2ClCH_2Cl were determined from the Patterson map. The structures of **4**—**8** were solved by direct methods (**4** and **6** by SHELXS-86[17] and **5**, **7**, and **8** by SIR-92[18]). Structure refinements were performed by using the teXsan crystallographic software package.[19] Scattering factors for neutral atoms were from Cromer and Waber[20] and anomalous dispersion[21] was included. X-Ray absorption for **2**·1.5CH_2ClCH_2Cl, **5**, and **8** was corrected by using the ψ-scan method.[22] Absorption corrections based on ψ-scans of **4** and **6** did not improve analyses [$R(F_o)$, $R_w(F_o)$, and GOF] and were not applied. An empirical absorption correction (DIFABS)[23] was applied to **7**.

In **2**·1.5CH_2ClCH_2Cl there are two independent solvate molecules, of which one is on an inversion center and the other is on a general site. The latter is disordered and the carbon atoms and one chlorine atom are split into two positions. The dichloroethane molecules in **4** are disordered and they were refined isotropically with restraint distances and angles. One of the solvent molecules in **8** is disordered and was refined similarly to those in **4**. Three independent *o*-dichlorobenzene molecules are included in **6**. Two of them located near a two-fold axis are disordered in a pair-wise manner over the sites related by the two-fold symmetry with the probability of one half. The carbon atoms of the disordered solvate molecules were refined by using a rigid model.

Crystal data and details of refinements for the structure determinations of **2**·1.5CH_2ClCH_2Cl and **4**—**8** are listed in Table 1.

Further details concerning the crystal structure investigation for (3,1)-[Rh_2(hq)$_4$py]·1.5CH_2ClCH_2Cl (CCDC No. 138223), (3, 1)-[Rh_2(mhq)$_4$(py)]PF_6·2CH_2ClCH_2Cl (CCDC No. 138224), (3, 1)-[Rh_2(hq)$_4$(py)]$SbCl_6$·CH_2Cl_2 (CCDC No. 138225), (3, 1)-[Rh_2(hq)$_4$(py)]PF_6·2*o*-$C_6H_4Cl_2$ (CCDC No. 138226), (3,1)-[Rh_2(hq)$_4$(py)]PF_6 (CCDC No. 138227), and (3,1)-[Rh_2(hq)$_4$(py)]-CF_3SO_3·2CH_2ClCH_2Cl (CCDC No. 138228) are available on request from the Director of the Cambridge Crystallographic Data Centre, 12 Union Road, Cambridge CB21EZ, (U.K.). The details of structures have been deposited as Document No. 73016 at the Office of the Editor of Bull. Chem. Soc. Jpn.

DFT Calculations. DFT calculations of π spin population distribution in hq radical were performed by using the Gaussian 94 program package.[24] The geometry of the radical, as a model for the bridging mhq and hq ligands in $\mathbf{1}^+$ and $\mathbf{2}^+$, was optimized by using the B3LYP[25—27] DFT method and the 6-31G basis set[28] with the O–C_2 and N–C_2 bond distances frozen at 1.30 and 1.35 Å, respectively, which are their average values in the crystal structures of $\mathbf{1}^+$ and $\mathbf{2}^+$ (For the numbering scheme of the carbon atoms, see Fig. 1c in a latter section). The π spin populations on C, N, and O atoms were evaluated for the geometry-optimized hq radical by following the scheme of the Mulliken population analysis.[29]

Results and Discussion

ESR of (3, 1)-[Rh_2(mhq)$_4$py]$^+$ (1^+) and (3, 1)-[Rh_2(hq)$_4$py]$^+$ (2^+). X-Band ESR spectra of $\mathbf{1}^+$ and $\mathbf{2}^+$ were observed for solutions of **3** and **5** in CH_2Cl_2 at 77 K. These spectra were rhombic, with the *g* tensors and the partially resolved Rh hyperfine splittings as listed in Table 2. The two principal values (g_1 and g_2) are similar each other and larger than the free electron value (g_e = 2.002), and g_3 is smaller than g_e for both of the cationic radicals. These characteristics show that odd electrons of these cationic radicals are accommodated in their δ^*_{RhRh} orbitals.[30] The axis of g_3 must be nearly parallel to the Rh–Rh bond.

^{1}H NMR of (3,1)-[Rh_2(mhq)$_4$py] (1). Since most of ^{1}H NMR peaks of cationic radical $\mathbf{1}^+$ were too broad to be observed and the assignments of the peaks were too difficult, we decided to estimate the paramagnetic shifts for the cationic radical from ^{1}H NMR spectra of mixtures of **1** and $\mathbf{1}^+$. A spectrum of a mixture should be an average of the spectra of **1** and $\mathbf{1}^+$ weighted with their mole fractions, due to rapid electron transfer between them. Extrapolations of the plots of the chemical shifts versus mole fraction would

Table 1. Crystallographic Data for (3,1)-[$Rh_2(hq)_4py$] (**2**·1.5CH_2ClCH_2Cl), (3,1)-[$Rh_2(mhq)_4(py)$]PF_6·2CH_2ClCH_2Cl (**4**), (3,1)-[$Rh_2(hq)_4(py)$]$SbCl_6$·CH_2Cl_2 (**5**), (3,1)-[$Rh_2(hq)_4(py)$]-PF_6·2*o*-$C_6H_4Cl_2$ (**6**), (3,1)-[$Rh_2(hq)_4(py)$]PF_6 (**7**), and (3,1)-[$Rh_2(hq)_4(py)$]CF_3SO_3·2CH_2ClCH_2Cl (**8**)

Compound	**2**·1.5CH_2ClCH_2Cl	**4**	**5**	**6**	**7**	**8**
Chemical formula	$C_{44}H_{35}Cl_3N_5O_4Rh_2$	$C_{49}H_{45}Cl_4F_6N_5O_4PRh_2$	$C_{42}H_{31}Cl_8N_5O_4Rh_2Sb$	$C_{53}H_{37}Cl_4F_6N_5O_4PRh_2$	$C_{41}H_{29}F_6N_5O_4PRh_2$	$C_{46}H_{37}Cl_4F_3N_5O_7SRh_2$
Formula weight	1009.96	1260.51	1280.92	1300.49	1006.49	1208.51
Space group	$P\bar{1}$ (2)	$P\bar{1}$ (2)	$P\bar{1}$ (2)	$C2/c$ (15)	$P2_12_12_1$ (19)	$P2_1/n$ (14)
a/Å	13.2649(9)	14.940(2)	12.892(3)	41.519(4)	17.073(3)	19.140(3)
b/Å	14.248(1)	17.052(2)	17.267(5)	11.419(3)	19.875(4)	11.278(3)
c/Å	11.2608(9)	10.793(1)	11.273(2)	23.963(3)	11.320(2)	23.450(3)
α/deg	104.891(7)	103.462(8)	107.62(2)	90	90	90
β/deg	95.478(7)	104.316(8)	95.66(2)	116.184(7)	90	111.58(1)
γ/deg	86.485(6)	101.181(9)	97.63(2)	90	90	90
V/Å^3	2046.0(3)	2497.1(6)	2344(1)	10194(2)	3841(1)	4707(1)
Z	2	2	2	8	4	4
T/°C	23	−40	23	−80	23	−80
ρ_{calc}/g cm^{-3}	1.639	1.676	1.814	1.695	1.740	1.705
Crystal size/mm	0.30 × 0.20 × 0.20	0.25 × 0.15 × 0.05	0.30 × 0.20 × 0.10	0.50 × 0.20 × 0.20	0.40 × 0.30 × 0.18	0.60 × 0.40 × 0.20
μ(Mo $K\alpha$)/cm^{-1}	10.51	9.78	17.67	9.61	9.79	10.39
Abs correction	ψ-scan	Not applied	ψ-scan	Not applied	DIFABS	ψ-scan
Range of 2θ/deg	4—55	4—55	4—55	4—55	4—60	4—55
Collected[a]	9820	11896	11144	12449	8748	11139
Unique[b]	6966	6166	5776[c]	7695	5462[d]	7561
Variables[e]	550	605	559	655	534	612
$R(F_o)$[f]	0.035	0.068	0.079	0.049	0.039	0.044
$R_w(F_o)$[g]	0.040	0.075	0.046	0.053	0.046	0.047
p[e]	0.020	0.020	0.005	0.025	0.020	0.020
Residual/e Å^{-3} [h]	−0.93, 1.11	−0.97, 1.32	−1.45, 1.56	−1.53, 0.89	−0.52, 0.60	−1.27, 1.08
GOF	1.55	1.68	1.65	1.54	1.74	1.77

a) Number of collected reflections. b) Number of unique reflections with $I > 2\sigma(I)$. c) Number of unique reflections with $I > 1.2\sigma(I)$. d) Number of unique reflections with $I > \sigma(I)$. e) Number of variables in the final refinement. f) $R = \Sigma||F_o| - |F_c||/\Sigma|F_o|$. g) $R_w = [\Sigma w(|F_o| - |F_c|)^2/\Sigma w|F_o|^2]^{1/2}$, $w = 1/[\sigma^2(F_o) + (p^2/4)]|F_o|^2$. h) Minimum and maximaum residual peaks in the final difference Fourier map: min, max.

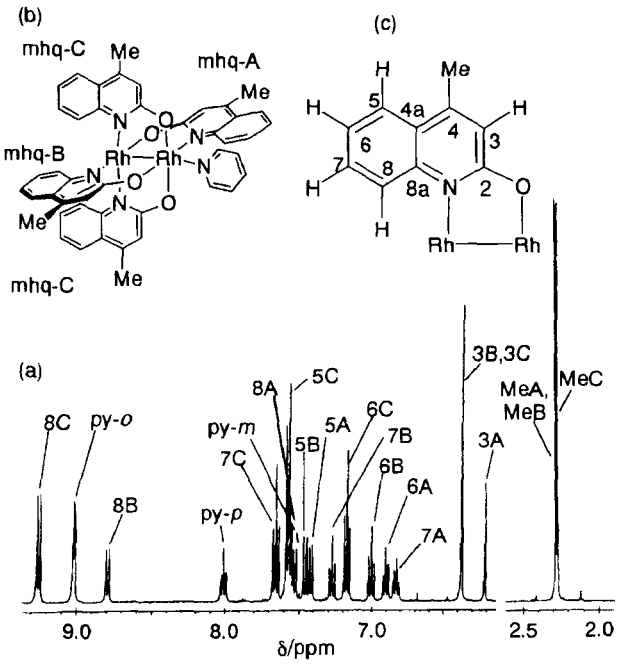

Fig. 1. ^{1}H NMR spectrum (400 MHz) of **1** in CD_2Cl_2 (a) with assignment (example: 3A denotes the resonance of proton 3 of the mhq-A ligand), the naming scheme for the mhq rings in **1** (b), and the numbering scheme for the carbon atoms in an mhq ligand (c).

Table 2. ESR Spin Hamiltonian Parameters for Frozen CH_2Cl_2 Solution (77 K) of (3,1)-$[Rh_2(mhq)_4py]^+$ ($\mathbf{1}^+$) and (3,1)-$[Rh_2(hq)_4py]^+$ ($\mathbf{2}^+$)

Radical	g_1	g_2	g_3	A_3(Rh)[a]/cm^{-1}
$\mathbf{1}^+$	2.123	2.093	1.922	1.99×10^{-3}
$\mathbf{2}^+$	2.123	2.093	1.923	2.05×10^{-3}

a) Two equibalent ^{103}Rh nuclei; splitting was resolved only in the direction of g_3.

yield both the paramagnetic shifts for $\mathbf{1}^+$ and their assignment based on that of the ^{1}H resonances of **1**.

Figure 1 shows the 400 MHz ^{1}H NMR spectrum of **1** in CD_2Cl_2 together with the assignment of the resonances based on the through-space correlations in NOESY spectra of **1**-d[5]. The assignment of the resonances of the pyridine ring protons are based on the comparison of spectra of **1** and **1**-d[5]. Among the resonances of 8A-, 8B-, and 8C-protons, that of the 8A site is abnormally shifted toward high field. This can be explained predominantly by the effect of the ring current of the axial pyridine, above the plane of which and in a short separation from which the 8A proton is located. Through-space correlation cross peaks were observed between the resonances of 8B- and 8C-protons in the NOESY spectra, contrary to the absence of correlation peaks of the 8A-proton resonance with either 8B- or 8C-proton resonances. The assignment of the resonances of the protons in the A and B rings is based on this identification of the 8A and 8B proton resonances and on the successive analyses of NOESY correlations starting from those involving 8A and 8B proton peaks.

The methyl proton resonance at 2.28 ppm was assigned to that of the C-mhq group, based on the result that the integrated area of this resonance corresponded to six equivalent protons even when paramagnetically shifted by successive additions of $\mathbf{1}^+$. The methyl proton peak at 2.27 ppm was assigned as the accidentally overlapping resonances for the A- and B-mhq ligands, and upon additions of $\mathbf{1}^+$ this peak split into two peaks, each corresponding to three equivalent protons.

Paramagnetic Shift in ^{1}H NMR of (3,1)-$[Rh_2(mhq)_4py]^+$ ($\mathbf{1}^+$). When small amounts of a CD_2Cl_2 solution of **3** was added successively to a sample of a CD_2Cl_2 solution of **1**, the ^{1}H resonances shifted in proportion to the mole fraction of the cationic radical, $x = [\mathbf{3}]/\{[\mathbf{1}]+[\mathbf{3}]\}$, as shown in Fig. 2. The shifts of the proton resonances from those of **1** induced by additions of the cationic radical salt are confirmed to be paramagnetic shifts by observation of linear dependence of the shifts on the reciprocal of the absolute temperature. By extrapolating the plots in Fig. 2 to $x = 1$, we obtained the paramagnetic shifts of $\mathbf{1}^+$ as listed in Table 3. The values in this table are the paramagnetic shifts defined as $\delta^P = \delta^+ - \delta^0$, where δ^+ and δ^0 denote a chemical shift of a resonance of $\mathbf{1}^+$ and of **1**, respectively. The assignment of the methyl proton resonances of the A- and B-mhq ligands in $\mathbf{1}^+$ remains uncertain, since these signals of **1** overlapped each other accidentally. We tentatively identify the methyl proton resonance with the most abnormal incline in the plots

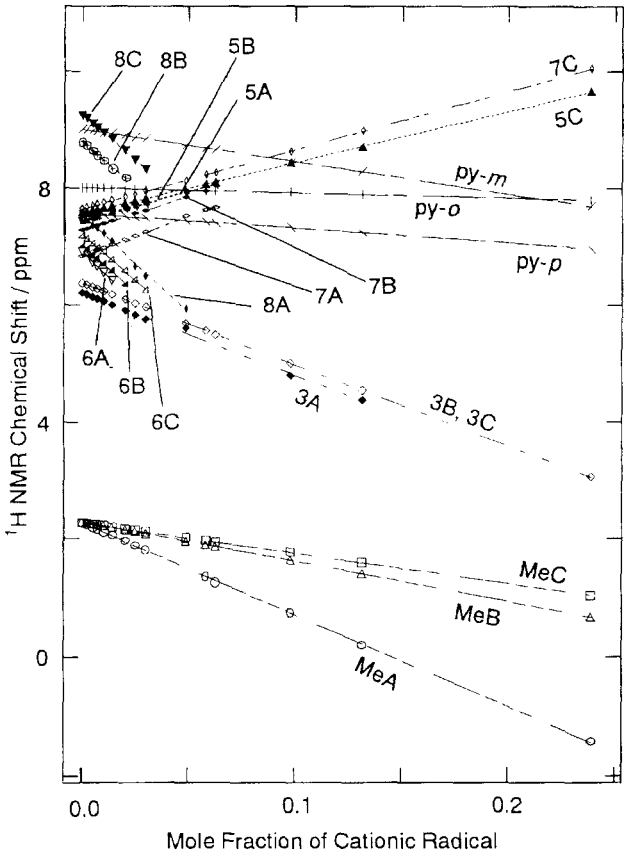

Fig. 2. Plots of shifts of 400 MHz ^{1}H resonance of mixtures of **1** and $\mathbf{1}^+$ against the mole fraction of $\mathbf{1}^+$ at 21 °C.

Table 3. Experimental Paramagnetic Shifts (δ^P/ppm) and Estimated Pseudo-Contact Shifts (δ^{PC}/ppm, in Parentheses) of ^{1}H Resonances of (3,1)-[Rh_2(mhq)$_4$py]$^+$ (**1**$^+$) at 21 °C

^{1}H Site[a)]	mhq-A	mhq-B	mhq-C		py
CH_3	−15.53	−5.17	−6.73	*o*-H	−5.55
	(0.41)	(0.40)	(0.41)		(−2.61)
H3	−14.14	−13.96	−13.96	*m*-H	−2.57
	(1.22)	(1.18)	(1.18)		(−0.94)
H5	10.47	9.87	8.79	*p*-H	−0.84
	(0.12)	(0.11)	(0.15)		(−0.77)
H6	−34.89	−31.78	−30.72		
	(−0.18)	(−0.22)	(−0.19)		
H7	13.85	11.70	10.09		
	(−0.63)	(−0.82)	(−0.82)		
H8	−33.41	−30.89	−30.88		
	(−2.54)	(−3.70)	(−3.86)		

a) See Fig. 1 for the naming scheme for the sites of the protons.

as that of the A-mhq group, because the mode of bridging of this mhq group differs from the others.

Spin Distribution in mhq Ligand of (3, 1)-[Rh_2(mhq)$_4$py]$^+$ (1$^+$). A paramagnetic shift is given as the sum of a contact shift (δ^C) and a pseudo-contact shift (δ^{PC}). The contact and pseudo-contact shifts of a doublet species with an axially symmetric g tensor are given by Eqs. 1 and 2, respectively:[31]

$$\delta^C = (a g_{iso}\mu_B)/(4kTg_H\mu_N) \quad (1)$$

$$\delta^{PC} = (\mu_0/4\pi)\{(g_{//}^2 - g_\perp^2)/(\mu_B^2/(12kT)\}\{(3\cos^2\theta - 1)/r^3\} \quad (2)$$

where the notations have the usual meanings.

We estimated the δ^{PC} for each of the protons of **1**$^+$ by using Eq. 2, principal values of its experimental g tensor, and the X-ray geometry of **4** (vide infra). We averaged the calculated δ^{PC} values for the protons of which the resonances were observed as equivalent. The g tensor values used for Eq. 2 were approximate ones given as $g_\perp = (1/2)(g_1+g_2)$ and $g_{//} = g_3$. The structure factors, $(3\cos^2\theta - 1)/r^3$, were calculated from the center of the Rh–Rh bond and from the Rh–Rh bond axis which is the parallel axis of the approximately axial g tensor. Thus estimated values of δ^{PC} listed in Table 3 were less than 10% of experimental δ^P values. Therefore the present approximation would not result in serious errors in the estimation of the contact shifts. By subtracting these estimated δ^{PC} values from the experimental δ^P values, we can estimate the values of δ^C as tabulated in Table 4. The proton isotropic hyperfine coupling constants, a, were evaluated as listed in Table 4 from δ^C by using Eq. 1. Since the odd electron in the δ^*_{RhRh} orbital is symmetry-forbidden to delocalize into the σ MOs of the bridging ligands in an idealized C_s geometry where the Rh–Rh bond is shared by the planes of the four bridging ligands, the π spin densities on the ring carbon atoms (ρ^π) of the bridging ligands can be estimated from the isotropic proton hyperfine coupling constants by using Eqs. 3 and 4:

for ring protons, $$a = Q_{CH}\rho^\pi \quad (3)$$

for methyl protons, $$a = Q_{Me}\rho^\pi \quad (4)$$

where the proportion constants of $Q_{CH} = -64$ MHz and $Q_{Me} = 76$ MHz were used. These Q-constant values are for aromatic π radicals.[32] The estimated π spin densities on carbon atoms of the mhq ligands are listed also in Table 4. The contact

Table 4. Estimation of Contact Shifts of Protons (δ^C/ppm) at 21 °C, Proton Hyperfine Coupling Constants (a/MHz, in Parentheses) and π Spin Densities $\langle\rho^\pi$, in Brackets $\rangle$ on Aromatic Carbon Atoms of (3,1)-[Rh_2(mhq)$_4$py]$^+$ (**1**$^+$)

^{1}H Site[a)]	mhq-A	mhq-B	mhq-C		py[b)]
CH_3	−15.9	−5.6	−7.1	*o*-H	−2.9
	(−0.58)	(−0.20)	(−0.26)		(−0.11)
	$\langle$ −0.0076 $\rangle$[c)]	$\langle$ −0.0027 $\rangle$[c)]	$\langle$ −0.0034 $\rangle$[c)]		
H3	−15.4	−15.1	−15.1	*m*-H	−1.6
	(−0.56)	(−0.55)	(−0.55)		(−0.06)
	$\langle$ 0.0087 $\rangle$	$\langle$ 0.0086 $\rangle$	$\langle$ 0.0086 $\rangle$		
H5	10.3	9.8	8.6	*p*-H	−0.07
	(0.38)	(0.35)	(0.31)		(−0.003)
	$\langle$ −0.0059 $\rangle$	$\langle$ −0.0055 $\rangle$	$\langle$ −0.0049 $\rangle$		
H6	−34.7	−31.6	−30.5		
	(−1.26)	(−1.15)	(−1.11)		
	$\langle$ 0.0197 $\rangle$	$\langle$ 0.0179 $\rangle$	$\langle$ 0.0173 $\rangle$		
H7	14.5	12.5	10.9		
	(0.53)	(0.46)	(0.40)		
	$\langle$ −0.0082 $\rangle$	$\langle$ −0.0071 $\rangle$	$\langle$ −0.0062 $\rangle$		
H8	−30.9	−27.2	−27.0		
	(−1.12)	(−0.99)	(−0.98)		
	$\langle$ 0.0175 $\rangle$	$\langle$ 0.0154 $\rangle$	$\langle$ 0.0153 $\rangle$		

a) For naming scheme of the sites, see Fig. 1. b) π Spin densities on carbon atoms of the axial pyridine have not been estimated due to the ambiguity in the mechanism of its proton hyperfine coupling. c) Spin density on the ring carbon atom to which the CH_3 group is bonded.

shifts of the axial pyridine have been estimated to be far smaller than those of the mhq protons. This is consistent with the idea that the δ^*_{RhRh} SOMO is symmetry-forbidden to mix with π or σ MOs of this ligand in an idealized arrangement of this ligand. The absolute values of the evaluated contact shifts for the axial pyridine protons are small and in the order of *o*-H > *m*-H > *p*-H. This also suggests that the spin distribution in this ligand cannot originate only from the odd electron delocalization into the pyridine π MOs allowed by the broken symmetry in the experimental geometry of the cationic radical.

Mechanism and Extent of Odd Electron Delocalization from δ^*_{RhRh} to π System of Bridging Ligands. The distribution of π spin population in neutral hq radical was calculated with the unrestricted B3LYP/6-31G method, as shown in Fig. 3. The SOMO of hq radical corresponds to the π HOMO of hq or mhq anionic ligand. The π spin densities on mhq carbon atoms of $\mathbf{1}^+$ in Table 4 were plotted versus the calculated π spin populations on the carbon atoms of hq radical, as shown in Fig. 4. The plots fit a line with the incline of 0.087, showing that the odd electron in the δ^*_{RhRh} orbital is delocalized predominantly into the π HOMOs of the four mhq ligands through the δ^*_{RhRh}–π_{bridge} orbital mixing, as depicted in Scheme 2, and that the extent of the delocalization is about 9% onto each of the bridging ligands. This analysis shows that the odd electron of cationic radical $\mathbf{1}^+$ or $\mathbf{2}^+$ is delocalized onto the 3-, 6-, 8-, and 4a-carbon atoms of the bridging mhq or hq ligands.

π-Stacking of Bridging Aromatic Ligands in Crystal. Figure 5 shows ORTEP views of $\mathbf{1}^+$ in **4** and $\mathbf{2}^+$ in **8**. The arrangements of the bridging ligands are distorted from an idealized C_s geometry in both of the cationic radicals. This is most probably due to the steric congestion of the hq or mhq ring hydrogen atoms on the C_{8B}, C_{8C}, and C_{8D} carbon

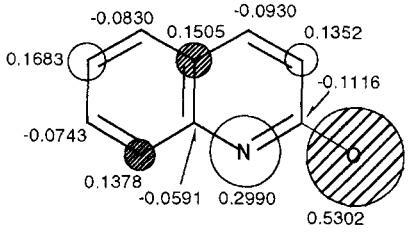

Fig. 3. π Spin populations in hq radical calculated with the B3LYP/6-31G method. White and hatched circles represent relative signs of its SOMO.

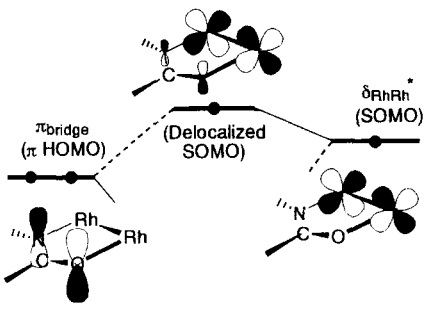

Scheme 2.

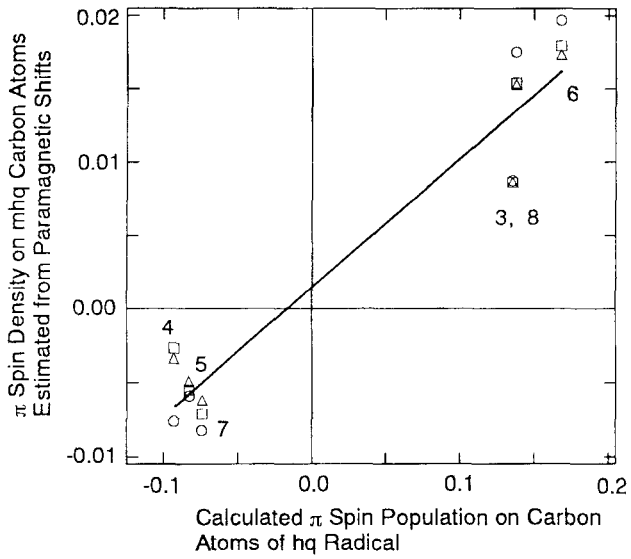

Fig. 4. Relation between π spin densities on mhq carbon atoms estimated from ^{1}H NMR paramagnetic shifts of $\mathbf{1}^+$ and π spin populations on carbon atoms of hq radical calculated by the B3LYP/6-31G method: circles for the A mhq ring, squares for the B mhq and triangles for the C ring. The numbers besides plots denote numberings of sites for carbon atoms in the hq radical and the mhq ligand. The line with the incline of 0.087 is the best fit to all of the plots.

atoms. Selected bond distances and angles of $\mathbf{1}^+$ in **4**, **2** in **2**·1.5CH_2ClCH_2Cl and $\mathbf{2}^+$ in **8** are listed in Table 5. The shortening of the RhN_{eq} and RhO bond lengths upon the one-electron oxidation of **2** is consistent with the idea that the oxidation removes an electron from the delocalized δ^*_{RhRh} orbital, which has RhN_{eq} and RhO π-antibonding character (Scheme 2).[11]

The crystal of **2**·1.5CH_2ClCH_2Cl consists of layers of molecules of **2** formed by intermolecular π-stacking of hq ligands. There exist three types of π-stack arrangements (Fig. 6). The shortest contacts in each type of the stack arrangements are 3.378(7), 3.364(7), and 3.528(7) Å. The 3.378(7) Å contact is between 3A and 6A′ carbon atoms (′ represents a neighboring molecule), on which high spin

Table 5. Selected Bond Distances (Å) and Angles (deg) of (3,1)-[Rh_2(mhq)$_4$(py)]$^+$ ($\mathbf{1}^+$)[a] in **4**, (3,1)-[Rh_2(hq)$_4$(py)] (**2**) in **2**·1.5CH_2ClCH_2Cl and $\mathbf{2}^+$ in **8**

Bond and Angle	**2**	$\mathbf{2}^+$	$\mathbf{1}^+$
Rh(1)–Rh(2)	2.3963(4)	2.3957(5)	2.402(1)
Rh(1)–O(1B)	2.029(3)	1.997(3)	1.988(4)
Rh(1)–O(1C)	2.018(3)	1.981(3)	1.995(6)
Rh(1)–O(1D)	2.024(3)	1.989(3)	1.977(6)
Rh(2)–O(1A)	2.033(2)	1.988(3)	1.974(4)
Rh(1)–N(1A)	2.081(3)	2.036(4)	2.036(5)
Rh(2)–N(1B)	2.040(3)	2.025(4)	2.020(5)
Rh(2)–N(1C)	2.068(3)	2.048(4)	2.034(6)
Rh(2)–N(1D)	2.054(3)	2.032(4)	2.043(6)
Rh(1)–N(1E)	2.140(3)	2.097(4)	2.111(7)
Rh(2)–Rh(1)–N(1E)	172.64(9)	170.9(1)	170.8(1)

a) Atom numbering scheme for **2** is same as that for $\mathbf{2}^+$ in Fig. 5b.

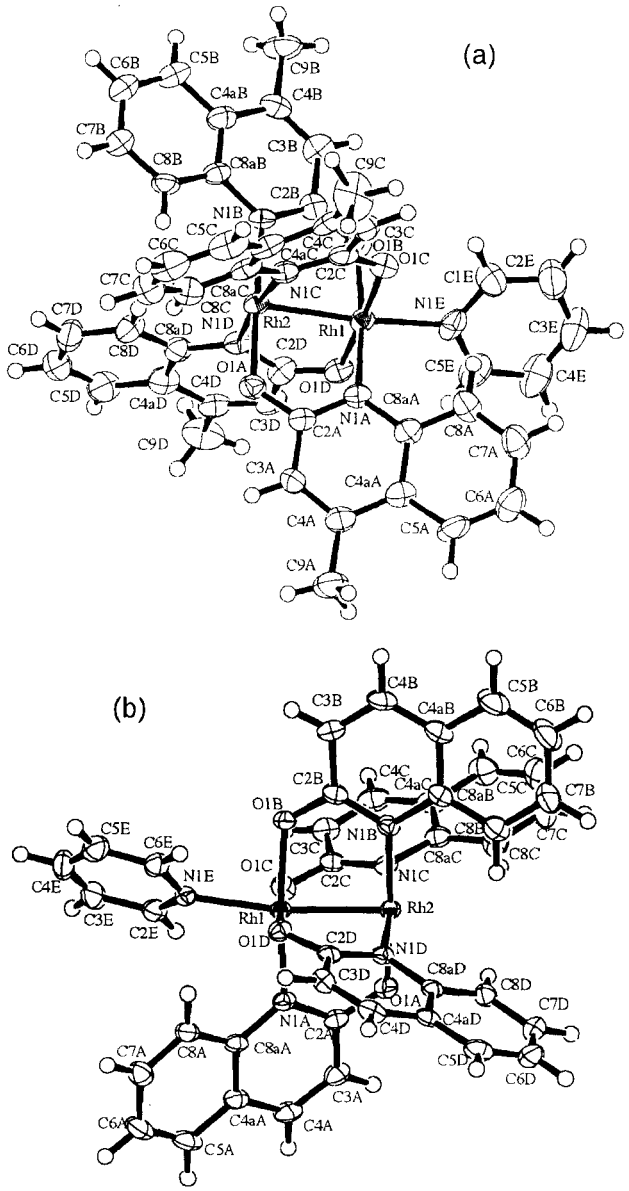

Fig. 5. ORTEP views 1^+ (a) in **4** and 2^+ (b) in **8** with the ellipsoids at the 50% probability level.

densities arise if the molecule is to be one-electron oxidized.

The shortest intermolecular contact between hq carbon atoms among the crystals of the current cationic radical salts was observed for **8**. The crystal consists of layers of 2^+ radicals alternately separated by a layer formed by the counter anions and solvate molecules. In the layer of 2^+ molecules, they form linear strings by π-stacking (Fig. 7d). The hq planes involved in the π-stacking are arranged crystallographically parallel. No π-stacking is observed between the strings. In the string, a 2^+ radical interacts with a neighboring radical through short contacts of $C_{6A}\cdots C_{3A'}$ and $C_{3A}\cdots C_{6A'}$ and with the other neighbor through contacts of $C_{8B}\cdots C_{6B''}$ and $C_{6B}\cdots C_{8B''}$. The carbon atoms involved in these shortest π-stack contacts have positive high spin densities.

The second shortest contact was observed in **5**. In this crystal the cationic radicals are arranged also to form sheets

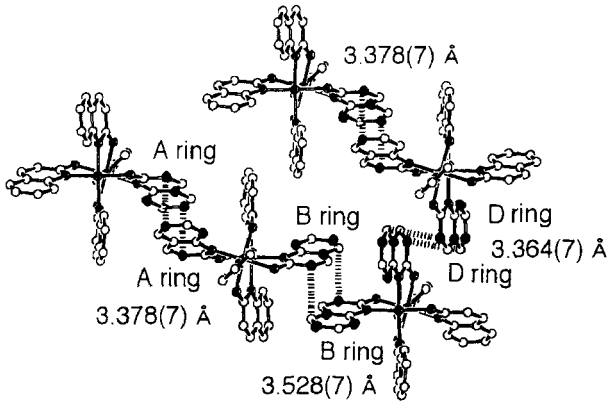

Fig. 6. π-Stacking in $2{\cdot}1.5CH_2ClCH_2Cl$; the solid circles on carbon atoms show the sites where 2^+ has positive high spin density.

of π-stacking alternately separated by a layer of counter anions and solvate molecules. Three hq bridges of each of 2^+ radicals stack over hq ligands of neighboring radicals, thus forming a two-dimensional π-stack network. The shortest contacts in each type of the π-stack arrangements in **5** are shown in Fig. 7a. One of the three types of the short contacts is between hq carbon atoms with positive spin densities (3A and 6A carbon atoms).

The 2^+ radical molecules in **6** (Fig. 7b) also form layers consisting of strings of a π-stack chain. The shortest contact is 3.56(1) Å and there is no short contact (< 3.7 Å) between high-spin-density hq carbon atoms.

The crystal of **7** consists of zigzag chains of π-stack arrangements of 2^+ radicals (Fig. 7c). Again there is no short contact (< 3.7 Å) between high-spin-density hq carbon atoms in the chain in this crystal. The shortest contact is 3.394(8) Å between the 4B and 8aC′ carbon atoms of hq ligands. The π-stack structure in this crystal does not have parallel arrangements even though all the arrangements of the π-stack pairs of hq ligands of neighboring molecules in $2{\cdot}1.5CH_2ClCH_2Cl$, **5**, **6**, and **8** are crystallographically parallel. Probably the absence of solvate molecules in the crystal of **7** reduced the freedom for parallel π-stacking of hq ligands that was otherwise possible.

Electronic Absorption Spectrum of Cationic Radical Salt. Figure 8 illustrates the electronic absorption spectra of nujol mulls of finely powdered crystalline salts of 2^+ and of its solution in CH_2ClCH_2Cl. The longest-wave-length band in the solution spectrum was observed as a shoulder at 1070 nm. All crystalline salts have bands with longer wave length than the longest-wave-length shoulder in the solution spectrum. The longest-wave-length shoulders or peaks of the crystalline salts are red-shifted in the order of **5** > **8** > **6** ≥ **7**. This trend is in parallel to the intermolecular short contacts of the carbon atoms with high π spin densities (3-, 4a-, 6-, and 8-carbon atoms), suggesting that the longest-wave-length band in solid-state spectra involves the intermolecularly interacting SOMO of the cationic radical.

Magnetic Susceptibility. To see intermolecular electron spin–spin interaction, we examined the temperature depen-

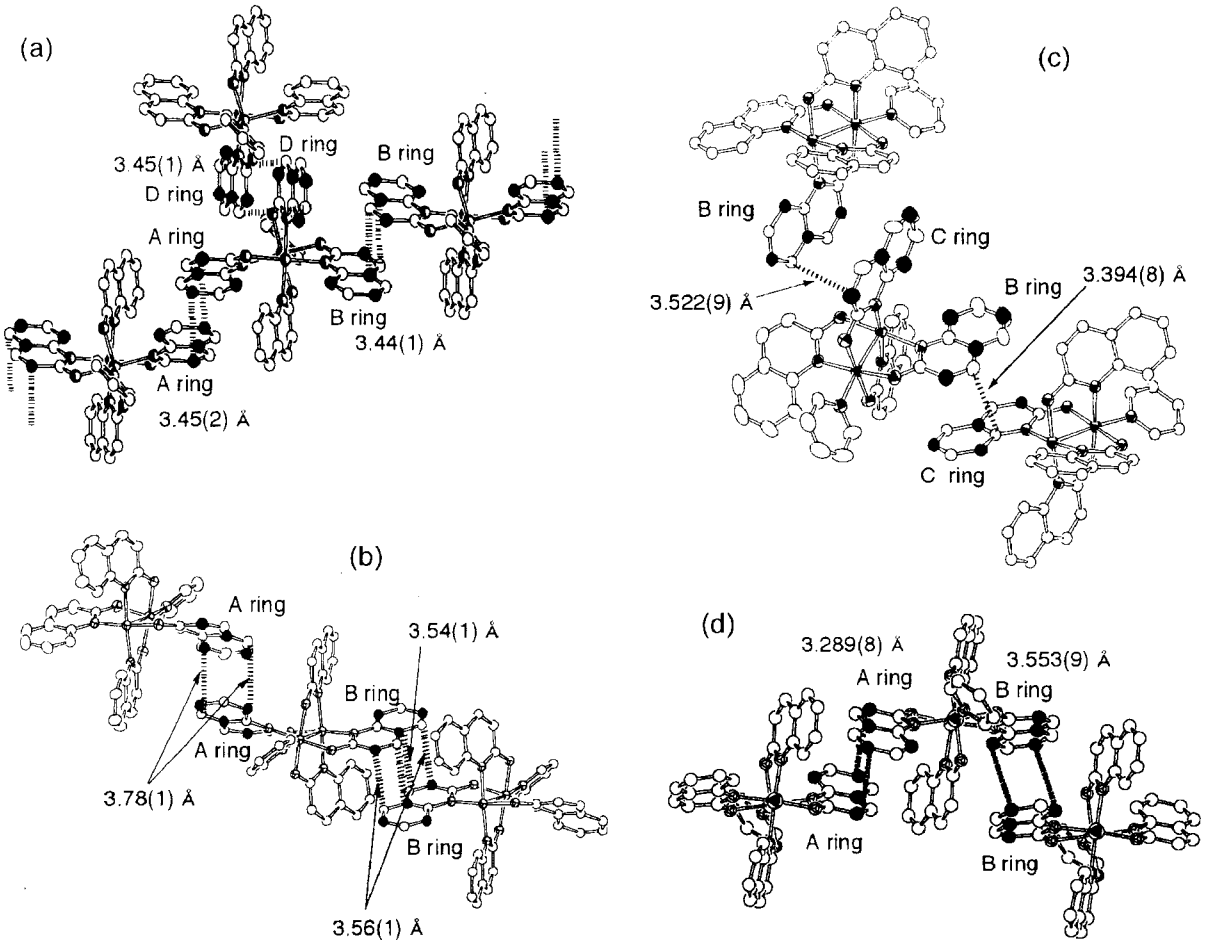

Fig. 7. π-Stacking of 2^+ in the crystals of **5** (a), **6** (b), **7** (c), and **8** (d); the carbon atoms with a solid circle have positive high spin density.

dence of magnetic susceptibilities of cationic radical salts (Fig. 9). The Curie–Weiss plots for **5**—**7** gave the parameters listed in Table 6. The susceptibility of **5** showed the largest deviation from the Curie law ($\theta = -12$ K) and that of **7** had the smallest Weiss constant. These results are in parallel to the conclusions that the packing structure of **5** has the shortest intermolecular contacts between high-spin-density hq carbon atoms among the present cationic radical salts and that the packing structure of **7** has no short contacts between high-spin-density carbon atoms. In a higher temperature range (> 150 K), **8** has a larger susceptibility than that expected from a Curie–Weiss fitting for lower temperatures. The deviation is 4×10^{-4} emu mol^{-1} at 200 K, exceeding the possible error in the diamagnetic correction by the Pascal method. We suppose that this arises also from the short contacts between high-spin-density hq carbon atoms in the crystal. The susceptibility of **6** in a high temperature range also deviates from the Curie–Weiss line, but the deviation is smaller than that of **8**, in parallel to rather long-distance contacts between the high-spin-density hq carbon atoms.

Table 6. Curie–Weiss Parameters[a] for (3,1)-$[Rh_2(hq)_4(py)]SbCl_6\cdot CH_2Cl_2$ (**5**), (3,1)-$[Rh_2(hq)_4(py)]PF_6\cdot 2o$-$C_6H_4Cl_2$ (**6**), and (3,1)-$[Rh_2(hq)_4(py)]PF_6$ (**7**)

Salt	Temp range[b]/K	μ/μ_B	θ/K
5	38 — 270	1.88	−12
6	4.2 — 270	1.94	−6
7	4.2 — 270	1.81	0.4

a) $1/\chi_{m,corr} = N_A\mu^2/[3k(T-\theta)]$. b) Temperature range for the Curie–Weiss fitting.

The temperature dependence of the magnetic susceptibility of **5** shows a peak (Fig. 10, circles) and we tried to reproduce this peak with two models. In the first model, we emphasize only the two-dimensional honeycomb arrangement of the cationic radicals formed by the π stacking in the crystal and neglect the difference among the local π stacking arrangements. A common magnetic interaction, $-2J$, was assumed to be induced between all the π-stacked pairs. We obtained $J = -8.58$ cm^{-1} ($= -12.3$ K) and $g_{eff} = 2.57$ by comparing the experimental maximum of the susceptibility with the theoretical one for the Heisenberg model of the honeycomb lattice of doublet molecules given by Navarro.[33] This value of g_{eff} is too large when compared with the g tensor obtained from ESR. The theoretical susceptibility obtained by using the high temperature series expansion for this model[33] gave the curve shown by the broken line in Fig. 10, which deviates appreciably from the observed values. In the

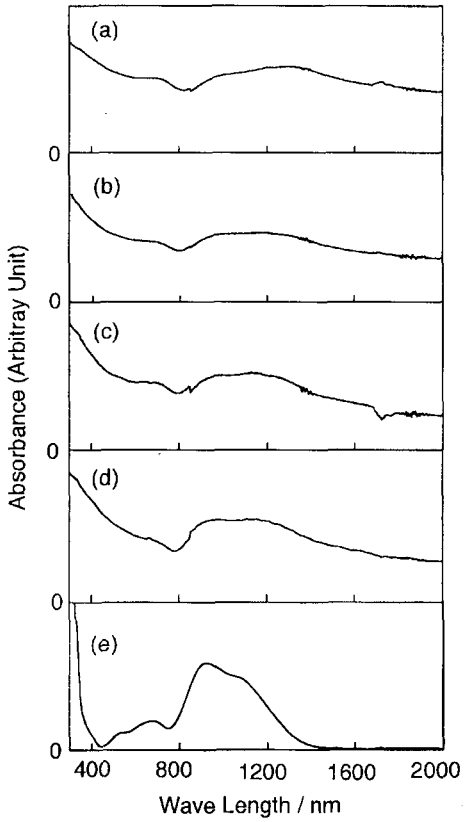

Fig. 8. Electronic absorption spectra of powdered crystalline salts (nujol mull) of **5** (a), **8** (b), **6** (c), and **7** (d), and the solution spectrum of **7** in CH_2ClCH_2Cl (e).

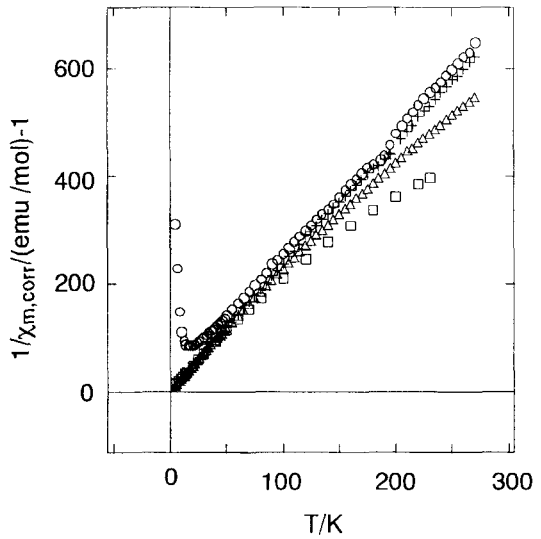

Fig. 9. Magnetic susceptibilities of **5** (circles), **6** (triangles), **7** (pluses), and **8** (squares).

second model, we emphasize that only one pair of the local π stack arrangement has intermolecular short contacts between high-spin-density carbon atoms and the others have no such intermolecular short contacts. The magnetic susceptibilities of **6** and **7** suggest that, without intermolecular short contacts between high-spin-density carbon atoms, π stacking does not induce large intermolecular magnetic interaction (i.e., $\theta \approx 0$

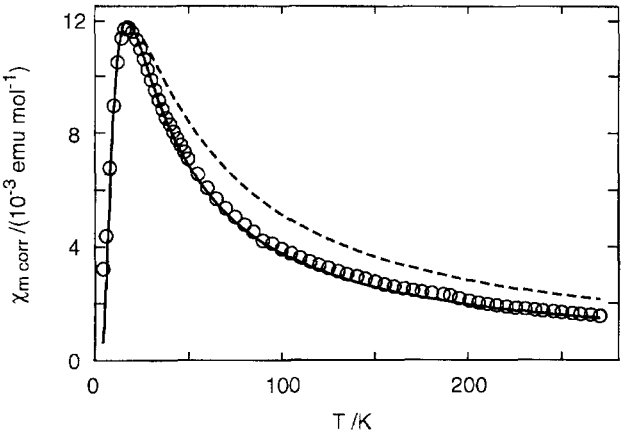

Fig. 10. Observed magnetic susceptibility of **5** (circles) and the best fit lines for the radical-dimer model with $J = -9.46$ cm^{-1} ($= -13.6$ K) and $\mu = 2.94$ B. M. ($g_{eff} = 2.08$ for the triplet dimer) (solid line), and for the Heisenberg model for the two-dimensional honeycomb lattice of $S = 1/2$ sites with $J = -8.58$ cm^{-1} ($= -12.3$ K) and $\mu = 2.22$ B.M. ($g_{eff} = 2.57$) (broken line).

K). Thus we analyzed the susceptibility of **5** by using a radical-pair model with the spin-spin interaction energy of $-2J$. This model gives the magnetic susceptibility as follows:[14]

$$\chi_m = N_A\mu^2/[2kT\{3+\exp(-2J/kT)\}] \quad (5)$$

where the notations have the usual meanings. A least-squares fitting of Eq. 5 to the susceptibility of **5** for the peak range ($8\ K < T < 50\ K$) gave $J = -9.46$ cm^{-1} ($= -13.6$ K) and $\mu/\mu_B = 2.94$, corresponding to $g_{eff} = 2.08$ for the triplet state of the dimer. Both the obtained value of g_{eff} and the magnetic susceptibility reproduced by these parameters (Fig. 10, solid line) are satisfactory. These results suggest that intermolecular short contacts between high-spin-density carbon atoms are important for magnetic interactions in the present type of complexes.

ESR of Crystalline Cationic Radical Salts. Figure 11 shows ESR spectra of powders of **8** and of a 1 : 1 (by mol) mechanical mixture of **8** and **2**·1.5CH_2ClCH_2Cl observed at 273 and 198 K. The spectra of powdered crystalline **8** are similar to the frozen solution spectrum of **8**, but with increased linewidth. The odd electrons in salt **8** do not hop or exchange

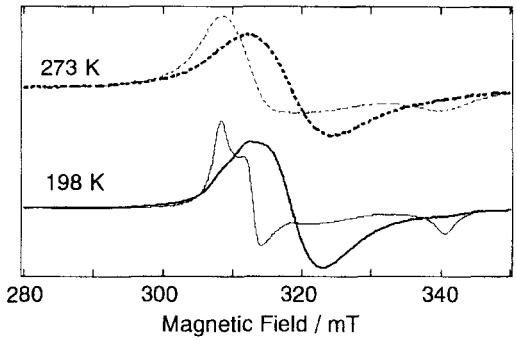

Fig. 11. X-band ESR spectra of powders of **8** (thin lines) and of a 1 : 1 (mol/mol) mechanical mixture of **8** and **2**·1.5CH_2ClCH_2Cl (thick lines) at 273 and 198 K.

over 2^+ molecules in the ESR time scale either at 273 or at 198 K. The spectrum of the mechanical mixture is isotropic, showing that the odd electrons in the mixture are hopping over Rh_2 units in the ESR time scale, averaging the orientation-dependent g factor into the observed isotropic one. There remains no odd electron which rests on one cationic radical molecule; otherwise we should have observed some anisotropic features in the spectra of the mixture. Since each of the particles in the powder is a single crystal orienting in one direction, the observation of an isotropic spectrum for the mechanical mixture indicates that odd electrons are hopping over particles of the radical salt as well as over dirhodium molecules in each of the particles. We suppose the effect of the mechanical mixing of the cationic radical salt crystal with the neutral complex crystal is doping of electrons into the radical salt crystal, inducing the hopping. The induced hopping of odd electrons in the mixed powder would have been made possible by the delocalization of the odd electrons in the δ^*_{RhRh} orbital onto the π system of the bridging ligands and then by the intermolecular π-stack interaction.

The X-ray powder diffraction pattern of the mechanical mixture did not show any new diffraction line other than those observed for the powders of **8** or **2**·1.5CH_2ClCH_2Cl. This shows that a new phase is not formed in the mechanical mixture within the detection limits of the measurement. The temperature dependence of the magnetic susceptibility of the mixture was examined by integrating the area of its ESR absorption; the result is shown in Fig. 12. The susceptibility is approximately linear to the inverse of temperature.

Electrical Conductivity. The electrical conductivity, $\log_{10}[\sigma/(S\,cm^{-1})]$, of pellets of **5**, **6**, **7**, and **8** at room temperature was in the order of 10^{-7} S cm^{-1}. The conductivity of the neutral complex, **2**·1.5CH_2ClCH_2Cl, was below 10^{-9} S cm^{-1} which is the lowest measurable limit of our apparatus.

Encouraged by the hopping of electrons in the mechanical mixture of crystals of the cationic radical salt and the neutral complex shown by the ESR study, we examined electrical conductivities of mechanically mixed powder of **7** and **8** with **2**·1.5CH_2ClCH_2Cl. Figure 13 displays the dependence of the conductivity on the ratio of the mixing of the complexes. Mechanical mixing of a small amount (ca. 20 mol%) of the neutral complex or a cationic radical salt into the other resulted in ca. 10^3 increase of the conductivity.

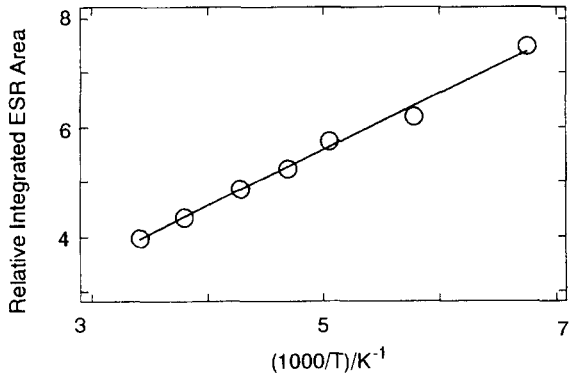

Fig. 12. Temperature dependence of the magnetic susceptibility of a 1 : 1 (mol/mol) mechanical mixture of **8** and **2**·1.5CH_2ClCH_2Cl measured as the integrated area of its ESR absorption.

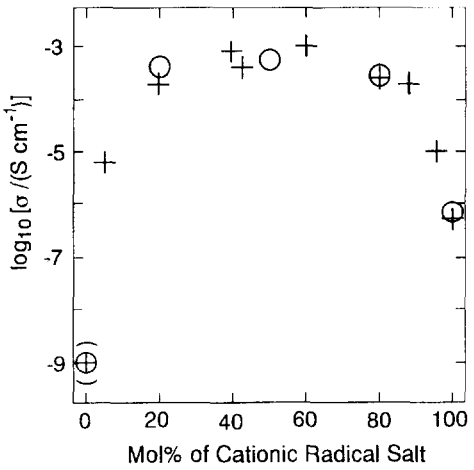

Fig. 13. Dependence of electrical conductivities of pellets at room temperature of **7** (circles) and **8** (pluses) mechanically mixed with **2**·1.5CH_2ClCH_2Cl on the mole fraction of the radical salt. The plots in the parentheses at 0 mol% are located at the lowest measurable limit.

We thank Professors Navarro (Zaragoza), Oshio (Sendai), and Ajiro (Fukuoka) for discussions on magnetic susceptibility. We thank Professors Yoshida and Funabiki (Kyoto) for measurements of powder X-ray diffraction. We are grateful to the Ministry of Education, Science, Culture and Sports of Japan for financial support. The DFT calculations were performed on the IBM SP2 workstation cluster at the computer center of the Institute for Molecular Science (Okazaki).

References

1 G. A. Rizzi, M. Casarin, E. Tondello, P. Piraino, and G. Gananozzi, *Inorg. Chem.*, **26**, 3406 (1987).

2 F. A. Cotton and X. Feng, *Inorg. Chem.*, **28**, 3042 (1989).

3 R. Cayton and M. H. Chisholm, *J. Am. Chem. Soc.*, **111**, 8921 (1989).

4 T. Kawamura, H. Katayama, H. Nishikawa, and T. Yamabe, *J. Am. Chem. Soc.*, **111**, 8156 (1989).

5 D. L. Lichtenberger, C. D. Ray, F. Stepniac, Y. Chen, and J. H. Weaver, *J. Am. Chem. Soc.*, **114**, 10492 (1992).

6 M. H. Chisholm, G. Christou, K. Folting, J. C. Huffman, C. A. James, J. A. Samuels, J. L. Wesemann, and W. H. Woodruff, *Inorg. Chem.*, **35**, 3643 (1996).

7 F. A. Cotton and A. Yokochi, *Inorg. Chem.*, **37**, 2723 (1998).

8 F. A. Cotton, L. M. Daniels, C. Lin, and C. A. Murillo, *J. Am. Chem. Soc.*, **121**, 4538 (1999).

9 T. Kawamura, H. Katayama, and T. Yamabe, *Chem. Phys. Lett.*, **130**, 20 (1986).

10 T. Kawamura, M. Ebihara, and M. Miyamoto, *Chem. Lett.*, **1993**, 1509.

11 T. Kawamura, M. Maeda, M. Miyamoto, H. Usami, K. Imaeda, and M. Ebihara, *J. Am. Chem. Soc.*, **120**, 8136 (1998).

12 B. G. Segal, M. Kaplan, and G. K. Fraenkel, *J. Chem. Phys.*, **43**, 4191 (1965).

13 M. Ebihara, M. Tsuchiya, M. Yamada, and T. Kawamura, *Inorg. Chim. Acta*, **231**, 35 (1995).

14 A. Earnshaw, "Introduction to Magnetochemistry," Academic, London (1968).

15 A. Weiss and H. Witte, "Magnetochemie," Verlag, Weinheim (1973).

16 G. A. Rempel, P. Legzdins, H. Smith, G. Wilkinson, and D. A. Ucko, *Inorg. Synth.*, **13**, 90 (1972).

17 G. M. Scheldrick, "SHELXS-86," Göttingen University (1986).

18 M. C. Burla, M. Camalli, G. Cascarano, C. Giacovazzo, G. Polidori, R. Spagna, and D. Viterbo, *J. Appl. Crystallogr.*, **22**, 398 (1989).

19 "Texsan, Single Crystal Structure Analysis Software, Version 1.6," Molecular Structure Corp., The Woodlands, TX (1993).

20 D. T. Cromer and J. T. Waber, in "International Tables for X-Ray Crystallography," Kynoch Press, Birmingham (1974), Vol. IV, Table 2.2A, pp. 71—98.

21 D. C. Creagh and W. J. McAuley, in "International Tables for X-Ray Crystallography," Vol. C, ed by A. J. C. Wilson, Kluwer Academic, Boston (1992), Table 4.2.6.8, pp. 219—222.

22 A. C. T. North, D. C. Phillips, and F. S. Mathews, *Acta Crystallogr., Sect. A*, **A24**, 351 (1968).

23 N. Walker and D. Stuart, *Acta Crystallogr., Sect. A*, **A39**, 158 (1983).

24 M. J. Frisch, G. W. Trucks, H. B. Schlegel, P. M. W. Gill, B. G. Johnson, M. A. Robb, J. R. Cheeseman, T. Keith, G. A. Petersson, J. A. Montgomery, K. Raghavachari, M. A. Al-Laham, V. G. Zakrzewski, J. V. Ortiz, J. B. Foresman, J. Cioslowski, B. B. Stefanov, A. Nanayakkara, M. Challacombe, C. Y. Peng, P. Y. Ayala, W. Chen, M. W. Wong, J. L. Andres, E. S. Replogle, R. Gomperts, R. L. Martin, D. J. Fox, J. S. Binkley, D. J. Defrees, J. Baker, J. P. Stewart, M. Head-Gordon, C. Gonzalez, and J. A. Pople, "Gaussian 94, Revision C.3," Gaussian, Inc., Pittsburgh (1995).

25 A. D. Becke, *J. Chem. Phys.*, **98**, 5648 (1993).

26 C. Lee, W. Yang, and R. G. Parr, *Phys. Rev. B*, **B37**, 785 (1988).

27 B. Miehlich, A. Savin, H. Stoll, and H. Preuss, *Chem. Phys. Lett.*, **157**, 200 (1989).

28 W. J. Hehre, R. Ditchfield, and J. A. Pople, *J. Chem. Phys.*, **56**, 2257 (1972).

29 R. S. Mulliken, *J. Chem. Phys.*, **23**, 1841 (1955).

30 T. Kawamura, K. Fukamachi, T. Sowa, S. Hayashida, and T. Yonezawa, *J. Am. Chem. Soc.*, **103**, 364 (1981).

31 I. Bertini and C. Luchinat, "NMR of Paramagnetic Molecules in Biological Systems," Benjamin/Cummings, Menlo Park, California (1986).

32 N. M. Atherton, "Electron Spin Resonance," Ellis Horwood, Chichester, U. K. (1973).

33 R. Navarro, in "Magnetic Properties of Layered Transition Metal Compounds," ed by L. J. de Jongh, Kluwer Academic, Dordrecht (1990), pp. 105—190.